ACS APPLIED MATERIALS & INTERFACES

RESEARCH ARTICLE

www.acsami.org

Effect of Nanoscale SubPc Interfacial Layer on the Performance of Inverted Polymer Solar Cells Based on P3HT/$PC_{71}BM$

Jung Yong Kim,[†] Seunguk Noh,[‡] Young Min Nam,[†] Jun Young Kim,[‡] Jeongkyun Roh,[‡] Myeongjin Park,[‡] Jason J. Amsden,[‡,§] Do Y. Yoon,[§] Changhee Lee,[*,‡] and Won Ho Jo[*,†]

[†]Department of Materials Science and Engineering, Seoul National University, 599 Gwanak-ro, Gwanak-gu, Seoul 151-742, Republic of Korea

[‡]School of Electrical Engineering and Computer Science, Inter-university Semiconductor Research Center, Seoul National University, 599 Gwanak-ro, Gwanak-gu, Seoul 151-744, Republic of Korea

[§]Department of Chemistry, Seoul National University, 599 Gwanak-ro, Gwanak-gu, Seoul 151-747, Republic of Korea

Supporting Information

ABSTRACT: The effect of a nanoscale boron subphthalocyanine chloride (SubPc) interfacial layer on the performance of inverted polymer solar cells based on poly (3-hexyl thiophene) (P3HT) and [6,6]-phenyl-C_{71}-butyric acid methyl ester (PC_{71}-BM) was studied. When a 1 nm SubPc layer was introduced between the active layer (P3HT:$PC_{71}BM$) and MoO_x in the device with ITO/ZnO/P3HT:$PC_{71}BM$/SubPc/MoO_x/Al configuration, the power conversion efficiency (PCE) was increased from 3.42 (without SubPc) to 3.59%. This improvement is mainly attributed to the enhanced open-circuit voltage from 0.62 to 0.64 V. When the Flory−Huggins interaction parameters were estimated from the solubility parameters through the contact angle measurement, it revealed that the interaction between SubPc and $PC_{71}BM$ is more attractive than that between SubPc and P3HT at the interface of P3HT:$PC_{71}BM$/SubPc, through which charges are well transported from the active layer to the anode. This is supported by a decrease of the contact resistance from 5.49 (SubPc 0 nm) to 0.94 MΩ cm (SubPc 1 nm). The photoelectron spectra provide another evidence for the enhanced PCE, exhibiting that the 1 nm thick SubPc layer extracts more photoelectrons from the active layer than other thicknesses.

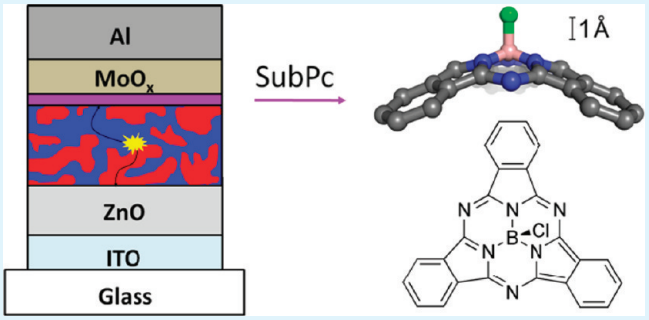

KEYWORDS: SubPc, interfacial layer, inverted polymer solar cells, poly(3-hexylthiophene):PCBM

INTRODUCTION

The power conversion efficiency (PCE) of polymer-based solar cells (PSCs) with conjugated polymer/fullerene bulk-heterojunction architecture has increased continuously over the past decade and reached about 8%.[1−3] The recent remarkable progress of PSCs has been made by molecular design and synthesis of new low bandgap conjugated polymers with appropriate energy levels and precise control of nanoscale morphology in active layer.[3−7] Considering this rapid advancement of PSCs, it is expected that the target PCE of 10% for commercialization of PSCs can be achieved in near future.[8] On the other hand, the stability of PSCs becomes increasingly important with development of new materials, because the commercially viable devices require not only high efficiency but also long-term stability.[9−13]

The inverted polymer solar cell has been extensively studied,[13−18] because it can eliminate the use of acidic poly(3,4-ethylene dioxythiophene):poly(styrene sulfonate) (PEDOT:PSS) in contact with indium tin oxide (ITO) as the hole transport layer and also allows the use of air sensitive metals as cathode.[16−18] It has been well-known that, in the standard organic photovoltaic device with an ITO/PEDOT:PSS/active layer/LiF/Al configuration, the acidic nature of PEDOT:PSS potentially etches an ITO electrode, resulting in an interfacial instability.[19] Another benefit of the inverted structure is to make it possible to use an air-stable high work function metal (e.g., Au, Ag) as the anode.[20] Furthermore, the inverted structure with a transparent buffer layer provides for a rich variety in device design including the possibility of a stacked tandem cell.[15,21,22]

Various materials have been used as interfacial layer: metals (Al, Ag, Au nanoparticle),[23] metal oxides (p-type: MoO_x, NiO, V_2O_5, WO_3; n-type: TiO_x, ZnO),[24−27] organic semiconductors (bathocuproine, bathophenathroline),[28] self-assembled monolayers (benzoic acid with negative dipole (−H, $-CH_3$, $-OCH_3$) or positive one ($-CF_3$, −CN, −SH)),[29,30] salts (Cs_2CO_3, LiF),[14,31] and others (polymer, polyelectrolyte).[32,33] When an interfacial layer is introduced into a PSC, it can significantly affect the open-circuit voltage (V_{oc}) by adjusting the energy barrier between two contact layers and also determine the device

Received: July 20, 2011
Accepted: October 4, 2011
Published: October 04, 2011

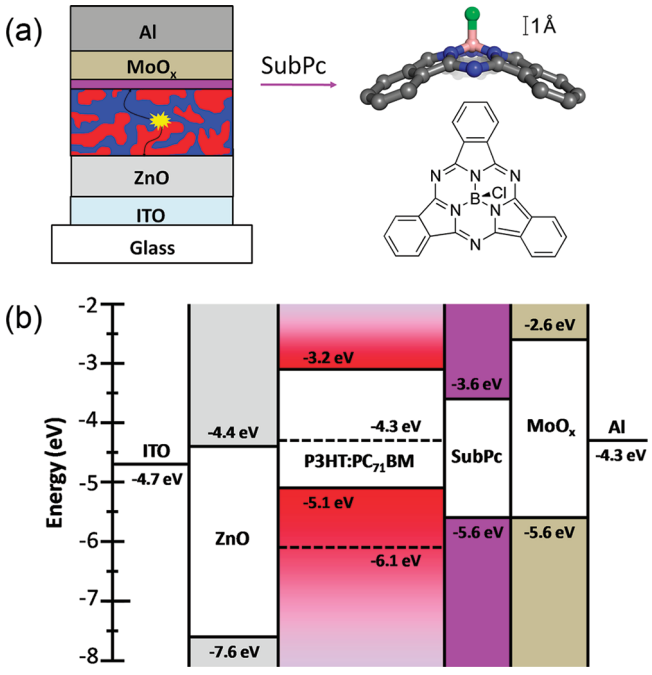

Figure 1. (a) Device architecture of the inverted polymer solar cell and chemical structure of SubPc (side and top views). (b) Energy level diagram.

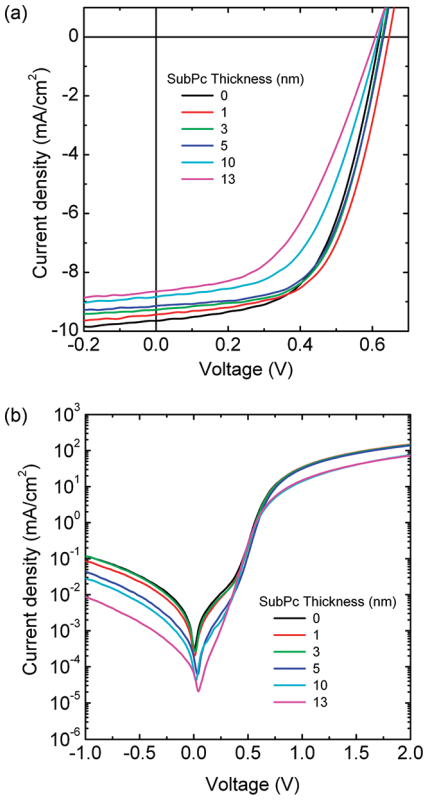

Figure 2. (a) Representative $J-V$ characteristics for the 95 nm thick P3HT:$PC_{71}BM$ = 1:0.8 (wt. ratio) solar cells with different thickness of the SubPc interfacial layer under simulated AM 1.5 spectrum. (b) Semilog $J-V$ curves of the solar cells in dark.

polarity by forming a selective contact for charge carriers (holes or electrons).[16−18,26,29] Furthermore, the layer acts as not only an optical spacer but also a protecting layer preventing direct chemical and physical reactions between the metal electrode and the active layer.[27]

In this study, we examined the electrical and optical effect of a boron subphthalocyanine chloride (SubPc) layer on the performance of inverted PSCs with a blend of poly (3-hexyl thiophene) (P3HT) and [6,6]-phenyl-C_{71}-butyric acid methyl ester (PC_{71}-BM) as an active layer. The device has an inverted structure with a configuration of ITO/ZnO/P3HT:$PC_{71}BM$/SubPc/MoO_x/Al, in which ZnO and MoO_x act as the electron and the hole selective layers, respectively. We used SubPc as an interfacial layer material, because SubPc has a strong dipole moment of 5.4−5.7 D and a deep highest occupied molecular orbital (HOMO) of −5.6 eV.[34,35] Thus, it is expected that the introduction of SubPc as an interfacial layer in the inverted PSCs enhances the photovoltage. To investigate the mechanism of this enhanced performance, the contact angle, the contact resistance, the surface morphology, and photoelectron spectra in air (PESA) were measured and analyzed.

MATERIALS AND METHODS

Materials. P3HT (M_n = 18 000 g/mol, M_w = 35 500 g/mol, polydispersity index = 1.9) was purchased from Rieke Metals. $PC_{71}BM$ and C_{60} were obtained from Nano-C. PEDOT:PSS (Baytron P VP Al 4083) and MoO_x were purchased from H. C. Starck and Serac Inc., respectively. Bathocuproine (BCP) and SubPc were obtained from Sigma-Aldrich Chemical Co. SubPc was purified by sublimation prior to use. ZnO nanoparticles with a wurtzite-type crystal structure were synthesized according to literature[36] and have an average diameter of 4.9 nm (see Figure S1 in the Supporting Information).

Fabrication of Inverted Polymer Solar Cell. The inverted polymer solar cell has a configuration of ITO/ZnO(40 nm)/P3HT:$PC_{71}BM$ (95 nm)/SubPc(0−13 nm)/MoO_x/Al. A patterned ITO glass with a sheet resistance of 10 Ω/□ was used as the substrate of device. The substrate was cleaned,using acetone, isopropyl alcohol and deionized water in an ultrasonic bath and then dried in an oven at 120 °C for 30 min. The ZnO dispersion (10 mg ZnO/1 mL butanol) was spin-coated on the ITO substrate in air at 2000 rpm for 60 s. Then the substrate was transferred into a glovebox, where 1.5 wt % polymer blend solution (P3HT:$PC_{71}BM$ (1:0.8 wt/wt) in *o*-dichlorobenzene (DCB)) was spin-coated on the top of ZnO/ITO substrate under N_2 at 1000 rpm for 30 s. The thickness of P3HT:$PC_{71}BM$ film was 95 nm as measured by the atomic force microscope (AFM). SubPc was evaporated at the rate of 0.5 Å/s with control of thickness (0−13 nm), and subsequently MoO_x was evaporated at the rate of 0.5 Å/s to deposit 10 nm. Finally aluminum was evaporated at the rate of 2−3 Å/s to deposit 100 nm in thickness on the top of MoO_3 film under the pressure of ∼1 × 10^{-6} Torr. The active area of device was 20 mm^2.

Fabrication of Field Effect Transistor. After hexamethyldisilazane (HMDS) liquid was spin coated on the top of the SiO_2 side of heavily doped *p*-type Si substrate sequentially at 500 rpm for 5 s and 2000 rpm for 7 s, a few drops of 0.3 wt % P3HT:$PC_{71}BM$ solution in DCB were spin-coated at 2000 rpm for 60 s under N_2 environment in a glovebox. The thickness of spin-coated P3HT:$PC_{71}BM$ film was about 20 nm. SubPc was evaporated at the rate of 0.5 Å/s to deposit 1−13 nm thickness, and subsequently MoO_x was evaporated at a rate of 0.5 Å/s to deposit 10 nm through a shadow mask. Finally source and drain electrodes with thickness of 50 nm were deposited by vacuum evaporation of Au through a shadow mask at a pressure of ∼1 × 10^{-6} Torr. The organic field effect transistor (FET) with Au/MoO_x/SubPc/P3HT:$PC_{71}BM$/HMDS/SiO_2/Si configuration, has a fixed channel width (W) of 1800 μm and various lengths (L) of 65, 95, and 110 μm.

Table 1. Photovoltaic Properties of Inverted Polymer Solar Cells As a Function of SubPc Thickness under White Light with Intensity of 100 mW/cm^2[a]

SubPc Thickness (nm)	0	1	3	5	10	13
J_{sc} (mA/cm^2)	9.71 (±0.10)	9.49 (±0.06)	9.13 (±0.20)	9.11 (±0.02)	8.88 (±0.02)	8.63 (±0.03)
V_{oc} (V)	0.62 (±0.00)	0.64 (±0.01)	0.63 (±0.01)	0.63 (±0.00)	0.61 (±0.01)	0.61 (±0.00)
FF	0.57 (±0.01)	0.60 (±0.01)	0.60 (±0.01)	0.59 (±0.01)	0.49 (±0.06)	0.40 (±0.08)
PCE (%)	3.42 (±0.02)	3.59 (±0.02)	3.47 (±0.02)	3.39 (±0.05)	2.63 (±0.30)	2.13 (±0.42)

[a] All the data are average values taken from measurements of at least 10 samples for each device.

Table 2. Parallel resistance (R_p) and series resistance (R_s) for inverted polymer solar cells as a function of SubPc thickness in dark. R_p and R_s are obtained at 0 and 1 V, respectively

	SubPc thickness (nm)					
	0	1	3	5	10	13
R_p (kΩ cm^2)	30.70 (± 4.23)	47.78 (± 7.82)	49.62 (± 12.13)	171.66 (± 15.81)	250.19 (± 19.38)	757.23 (± 52.83)
R_s (Ω cm^2)	10.25 (± 1.30)	9.53 (± 1.12)	9.68 (± 1.71)	9.96 (± 1.65)	23.50 (± 8.01)	28.41(± 7.40)

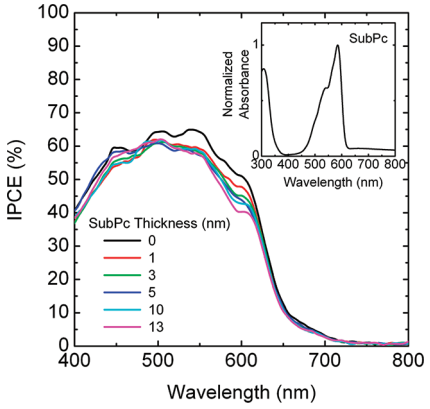

Figure 3. IPCE curves of polymer solar cells with different SubPc layer thickness. Inset represents normalized absorption spectrum of an evaporated SubPc film.

Table 3. Contact Angle (water), Surface Energy, and Solubility Parameter

materials	contact angle (deg)	surface energy (mJ/m^2)	solubility parameter (J/cm^3)$^{1/2}$
P3HT	99.28	22.74	17.86
$PC_{71}BM$	75.74	37.56	22.97
P3HT:$PC_{71}BM$	84.99	33.45	21.67
SubPc	81.20	34.09	21.88

Characterization. Molecular weight of P3HT and its distribution were measured by gel permeation chromatography (GPC) (PL-GPC50) equipped with a refractive index detector using THF as an eluent. The columns were calibrated using standard polystyrene samples. Thermal properties were measured using differential scanning calorimetry (DSC) (TA Instruments, DSC-Q1000) with a scan rate of 10 °C/min under N_2 atmosphere. Contact angles of water were determined on the evaporated SubPc and other spin-coated films (P3HT, $PC_{71}BM$, and P3HT:$PC_{71}BM$ blend) using a contact angle analyzer (Phoenix 300+/LCA10). Optical absorption was measured by an ultraviolet-visible-near-infrared (UV-vis-NIR) spectrophotometer (Lambda 850, Perkin-Elmer). Reflectance of devices was measured by a spectrophotometer (Cary5000, Varian). Tapping-mode AFM images were taken with Seiko Instrument (SPA-400). Scanning electron microscopy (SEM) images were obtained with JSM 5410LV, which is equipped with energy dispersive X-ray spectroscopy (EDS) for elemental analysis (see Figures S2−5 in the Supporting Information). Transmission electron microscopy (TEM) images were obtained at 80 kV with a JSM 5410LV (JEOL) (see Figure S6 in the Supporting Information). For TEM samples, a spin-coated P3HT:$PC_{71}BM$ film on the PEDOT:PSS-coated glass substrate was immersed into deionized water, and the spin-coated film was then floated onto the water and collected by a 300 mesh copper grid. Refractive index (n) and extinction coefficient (k) of materials were measured using a spectroscopic ellipsometer (M2000D, Woollam). Ionization potential (~4.8−5.1 eV) of P3HT was measured by a photoelectron spectrometer in air (PESA: Model AC-2, RKI instruments), where samples

Table 4. Flory−Huggins Interaction Parameters at T = 298 K

binary pair	χ_{ij}
P3HT/$PC_{71}BM$	1.19
P3HT/SubPc	0.75
$PC_{71}BM$/SubPc	0.05

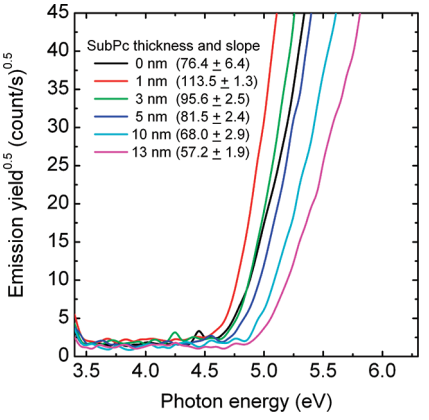

Figure 4. Photoelectron spectra for the SubPc/P3HT:$PC_{71}BM$ (= 95 nm)/glass with different SubPc thickness.

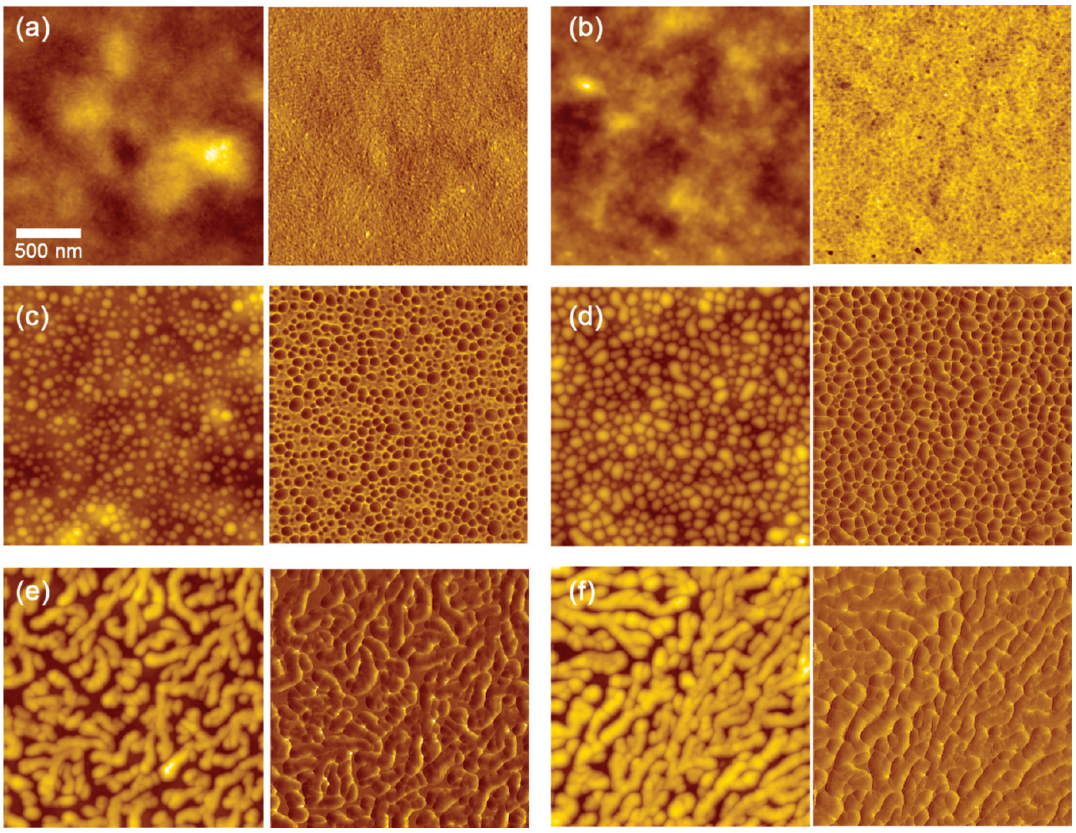

Figure 5. AFM tapping mode height (left column) and simultaneously acquired phase image (right column) of SubPc/P3HT:$PC_{71}BM$(= 95 nm)/Glass: (a) SubPc= 0 nm, (b) SubPc= 1 nm, (c) SubPc= 3 nm, (d) SubPc= 5 nm, (e) SubPc= 10 nm, and (f) SubPc= 13 nm. All the images are $2 \times 2\ \mu m^2$. Image height range, maximum peak-to-valley is 35 nm (SubPc = 0−1 nm), 40 nm (SubPc = 3−5 nm), and 50 nm (SubPc = 10−13 nm).

with a configuration of SubPc (0−13 nm)/P3HT:$PC_{71}BM$ (1:0.8 wt/wt, 95 nm)/glass were used. Electrical characterization of transistor was performed in the dark using a semiconductor parameter analyzer (HP 4155 C) under N_2 in a glovebox. The total device resistance [$R_{tot} = R_{chan}$ (channel resistance) + R_c (contact resistance)] was obtained in the linear regime of the output characteristics at the gate voltage (V_G) of −80 V, and the R_c (= the sum of source and drain resistances) was estimated by linearly extrapolating the transmission line (R_{tot} vs L) to L = 0. White Xe light (300 W, Oriel) with an intensity of 100 mW/cm^2 (simulated AM 1.5G spectrum) was used for PSCs. Current density−voltage (J−V) characteristics of devices were measured with a Keithley 237 source measurement unit controlled by LabView code. Photocurrent action spectra were obtained using a monochromator (Cornerstone) with commercially available gratings and filter (Newport).

RESULTS AND DISCUSSION

Figure 1 shows the configuration of an inverted polymer solar cell with an interlayer of SubPc and the schematic energy diagram based on the Schottky-Mott-like interface,[13,37] where ZnO and MoO_x act as the electron and the hole selective layers, respectively, determining the electrode polarity of device. It has already been known that the charge transfer across the cathode-side interface between fullerene and ZnO is facile because of their negligible energy barrier for electrons.[37] In this work, we have focused on the anode-side interface between P3HT and MoO_x and modified the interface for improving the PCE by introducing a pyramidal-shaped SubPc molecule as an interfacial layer.

Figure 2 shows the J−V characteristics for the inverted polymer solar cells with different SubPc thickness under simulated AM1.5G illumination and in the dark, and their photovoltaic properties are summarized in Tables 1 and 2. As shown in Figure 2a and Table 1, the short-circuit current density (J_{sc}) monotonically decreases with increasing the SubPc thickness, whereas V_{oc} and fill factor (FF) show a maximum at 1 nm and 3−5 nm thick SubPc layers, respectively. Especially, the increase in V_{oc} from 0.62 (without SubPc) to 0.64 V (SubPc 1 nm) is noteworthy: the V_{oc} of 0.64 V is one of the highest recorded values for polymer solar cells based on P3HT:PCBM. As a result, the PCE is improved from 3.44% (the reference device without SubPc) to 3.62% (1 nm SubPc). When the parallel (R_p) and the series resistances (R_s) of device are measured, it reveals that R_s exhibits low values (∼10 Ω cm^2) at 0−5 nm SubPc, while R_p gradually increases with increasing the SubPc thickness, as shown in Table 2, indicating that the solar cell with a SubPc layer of 1 nm thickness shows the best diode.

Figure 3 shows the incident photon to current efficiencies (IPCE) of devices with different SubPc thickness, which resembles the shape of the UV−vis absorption and the reflectance spectra in Figure S7 in the Supporting Information. The IPCE decreases slightly with increasing the SubPc thickness, which corresponds to the decrease of J_{sc} with increasing the SubPc thickness. It should be noted here that the absorption of SubPc barely contributes to the photocurrent generation, because the IPCEs of devices with SubPc layer do not exhibit a peak at 582 nm, corresponding to the maximum absorption wavelength

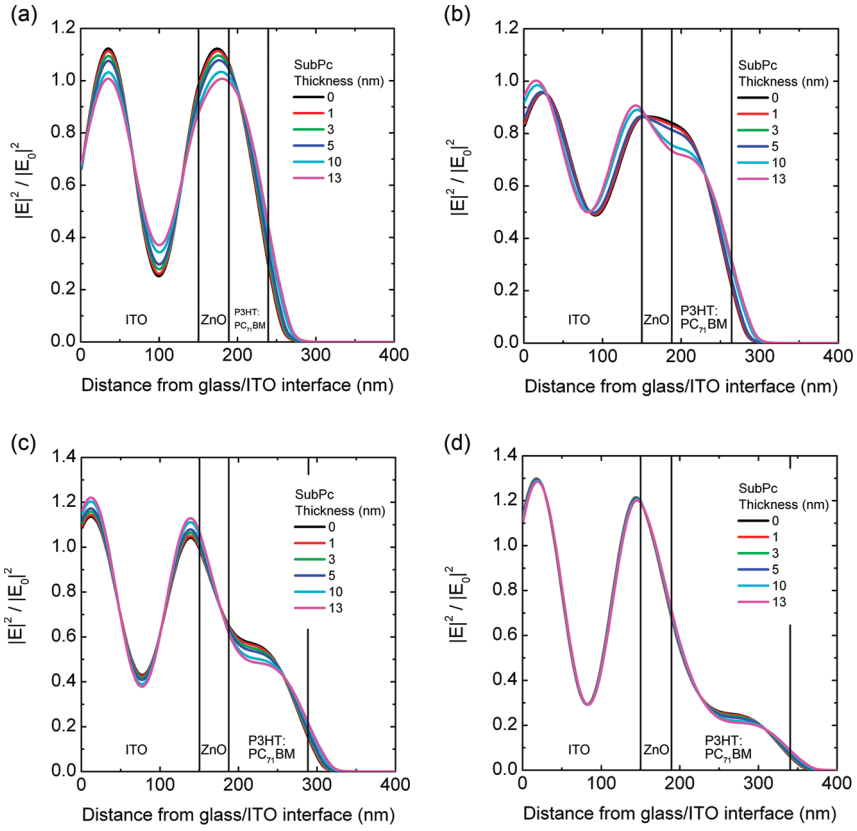

Figure 6. Calculated optical electric field for the monochromatic light at the wavelength of 500 nm in a device with the thickness of active layer (P3HT:$PC_{71}BM$ = 1:0.8 wt. ratio): (a) 50, (b) 75, (c) 100, and (d) 150 nm, in each of which the thickness of SubPc layer is varied from 0 to 13 nm.

of SubPc (the inset of Figure 3; see also Figure S7b in the Supporting Information).

To investigate the reason why the 1 nm thick SubPc affords the largest V_{oc} in device, we estimate first the binary interaction energies between P3HT, $PC_{71}BM$, and SubPc. For the purpose, we measured contact angles of water on spin-coated films, from which the surface energies are calculated by using the Li and Neumann's relation.[38] The solubility parameter (δ) is then calculated from the surface energy according to the method previously reported.[39] To this end, the Flory−Huggins interaction parameter (χ_{ij}) between components i and j was calculated from the relation of $\chi_{ij} = \hat{V}_1 R^{-1} T^{-1} (\delta_i - \delta_j)^2$, where $\hat{V}_1$ is a molar volume of solvent defining the lattice size, R is the gas constant, and T is a temperature. The results are summarized in Tables 3 and 4. Since the smaller value of χ_{ij} indicates stronger attractive interaction between two components, it is realized that the strength of attractive interaction is on the order of $PC_{71}BM$/SubPc > P3HT/SubPc > P3HT/$PC_{71}BM$, as can be seen in Table 4. Hence, it is expected that SubPc molecules have stronger interaction with $PC_{71}BM$ domain than with P3HT domain. Hence, when SubPc molecules are deposited on the top of phase-separated P3HT:$PC_{71}BM$ blend film, the preferential interaction (or wetting) exists between SubPc and $PC_{71}BM$ (or $PC_{71}BM$-rich phase) at the interface, through which charges are well transported from the active layer to the anode (MoO_x/Al). This is evidenced by significant reduction of the contact resistance from 5.49 (SubPc 0 nm) to 0.94 MΩ cm (SubPc 1 nm) (see Figure S8 in the Supporting Information).

Figure 4 shows photoelectron spectra for the samples with the SubPc (0−13 nm)/P3HT:$PC_{71}BM$ (95 nm)/glass configuration. Since the steeper slope of emission-yield line indicates more efficient extraction of photoelectrons, it is expected that the 1 nm thick SubPc layer transports charges more effectively than the reference device without SubPc, although J_{sc} decreases simply with increasing the SubPc layer (Table 1), which will be explained later by the optical simulation. When the thickness of SubPc layer is further increased, the slope becomes smaller than the reference, indicating that the extraction of photoelectrons becomes less efficient due to substantial increase of series resistance (see Table 2).

When the surface AFM images of film with different SubPc thickness are examined, as shown in Figure 5, it reveals that the films with SubPc 0 nm and SubPc 1 nm have smooth surface while the SubPc films with 3−5 nm and 10−13 nm thicknesses show circular domains with average diameter of 70−80 nm and rugged oblong shaped domains, respectively.

The optical effect of SubPc layer on the performance of device was examined by the computer simulation based on the transfer matrix combined with the complex refractive index of each layer (Figures S9−S11 in the Supporting Information).[40] Figure 6 shows the change of optical electric field distribution in the device at the wavelength of 500 nm with varying the SubPc thickness for each of four different active layer thicknesses. A local optical maximum of profile is observed in the active layer with the thickness of 75−100 nm, indicating that the optimum thickness of active layer lies in the range of 75−100 nm, whereas the optical electric field becomes much smaller in the thicker

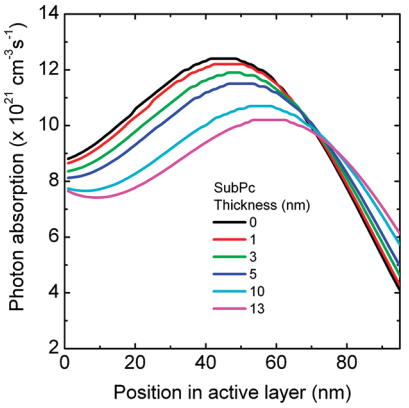

Figure 7. Calculated optical electric field for the white light (wavelength of 350−800 nm) in an active layer (P3HT:$PC_{71}BM$ = 1:0.8 wt. ratio) with a thickness of 95 nm, in which the thickness of SubPc layer is varied from 0 to 13 nm.

active layer (150 nm). When one takes into account the overall wavelength (350−800 nm) for calculation of the optical electric field distribution, as shown in Figure 7, the optical profile in the 95 nm thick active layer shows that the amount of photon absorbed decreases with increasing the SubPc thickness, and the maximum absorption shifts toward the active layer/SubPc interface. Therefore, an increase in SubPc layer thickness may unfavorably affect the current density J_{sc}, as can be seen in Table 1.

CONCLUSION

When a 1 nm SubPc interfacial layer was introduced between the active layer (P3HT:$PC_{71}BM$) and MoO_x, the PCE was increased from 3.42 to 3.59%, which is attributed mainly to enhancement of V_{oc} from 0.62 to 0.64 V. This V_{oc} value (0.64 V) is one of the highest records for polymer solar cells based on P3HT:PCBM. First, the enhancement of V_{oc} arises primarily from a decrease of R_s from 10.25 (SubPc 0 nm) to 9.53 Ω cm^2 (SubPc 1 nm) and with an increase of R_p from 30.70 to 47.78 kΩ cm^2. Second, the Flory−Huggins interaction parameter explains stronger interaction (or wetting) between SubPc and $PC_{71}BM$ than between SubPc and P3HT at the interface, through which charges are well transported from the active layer to anode, as evidenced by a decrease of the contact resistance from 5.49 (SubPc 0 nm) to 0.94 MΩ·cm (SubPc 1 nm). Third, the PESA shows that 1 nm thick SubPc layer extract more photoelectrons from the active layer than other thicknesses, indicating better charge transport at the interface in the presence of 1 nm SubPc. Although the optical simulation using the transfer matrix predicts that the short-circuit current density decreases with increasing the thickness of SubPc layer, the decrease is not so significant when a few nanometer thick layer is used.

ASSOCIATED CONTENT

Supporting Information. XRD pattern, SEM images with EDS spectra, TEM image, DSC data, UV−vis absorption/reflectance spectra, $J-V$ curve and IPCE data for the SubPc:C_{60} bilayer solar cell, transmittance line plot for contact resistance, complex refractive index data by spectroscopic ellipsometer, and calculated optical electric field in active layer with varying thickness. This material is available free of charge via the Internet at http://pubs.acs.org.

AUTHOR INFORMATION

Corresponding Author

*E-mail: whjpoly@snu.ac.kr (W.H.J.); chlee7@snu.ac.kr (C.L.).

ACKNOWLEDGMENT

The authors thank the Ministry of Education, Science and Technology (MEST), Korea, for financial support through the Global Research Laboratory (GRL), Acceleration Research (R0A-2008-000-20108-0), and BK21 programs. J.J.A. is funded by a National Science Foundation International Research Fellowship (OISE-0965057).

REFERENCES

(1) Yu, G.; Gao, J.; Hummelen, J. C.; Wudl, F.; Heeger, A. J. *Science* **1995**, *270*, 1789–1791.
(2) Halls, J. J. M.; Walsh, C. A.; Greenham, N. C.; Marsegila, E. A.; Friend, R. H.; Moratti, S. C.; Holmes, A. B. *Nature* **1995**, *376*, 498–500.
(3) See Solarmer press release 2010, www.solarmer.com.
(4) Chen, H.-Y.; Hou, J.; Zhang, S.; Liang, Y.; Yang, G.; Yang, Y.; Yu, L.; Wu, Y.; Li, G. *Nat. Photonics* **2009**, *3*, 649–653.
(5) Liang, Y.; Yu, L. *Acc. Chem. Res.* **2010**, *43*, 1227–1236.
(6) Chu, T.-Y.; Lu, J.; Beaupre, S.; Zhang, Y.; Pouliot, J.-R.; Wakim, S.; Zhou, J.; Leclerc, M.; Li, Z.; Ding, J.; Tao, Y. *J. Am. Chem. Soc.* **2011**, *133*, 4250–4253.
(7) Price, S. C.; Stuart, A. C.; Yang, L.; Zhou, H.; You, W. *J. Am. Chem. Soc.* **2011**, *133*, 4625–4631.
(8) Scharber, M. C.; Muehlbacher, D.; Koppe, M.; Denk, P.; Waldauf, C.; Heeger, A. J.; Brabec, C. J. *Adv. Mater.* **2006**, *18*, 789–794.
(9) Jørgensen, M.; Norrman, K.; Krebs, F. C. *Sol. Energy Mater. Sol. Cells* **2008**, *92*, 686–714.
(10) Hsieh, C.-H.; Cheng, Y.-J.; Li, P.-J.; Chen, C.-H.; Dubosc, M.; Liang, R.-M.; Hsu, C.-H. *J. Am. Chem. Soc.* **2010**, *132*, 4887–4893.
(11) Norman, K.; Madsen, M. V.; Gevorgyan, S. A.; Krebs, F. C. *J. Am. Chem. Soc.* **2010**, *132*, 16883–16892.
(12) Griffini, G.; Douglas, J. D.; Piliego, C.; Holcombe, T. W.; Turri, S.; Fréchet, J. M. J.; Mynar, J. L. *Adv. Mater.* **2011**, *23*, 1660–1664.
(13) Sun, Y.; Seo, J. H.; Takas, C. J.; Seifter, J.; Heeger, A. J. *Adv. Mater.* **2011**, *23*, 1679–1683.
(14) Liao, H.-H.; Chen, L.-M.; Xu, Z.; Yang., Y. *Appl. Phys. Lett.* **2008**, *92*, 173303–3.
(15) Hau, S. K.; Yip, H.-L.; Chen, K.-S.; Zou, J.; Jen, A. K.-Y. *Appl. Phys. Lett.* **2010**, *97*, 253307–3.
(16) Chen, L.-M.; Hong, Z.; Li, G.; Yang., Y. *Adv. Mater.* **2009**, *21*, 1434–1449.
(17) Steim, R.; Kogler, F. R.; Brabec, C. J. *J. Mater. Chem.* **2010**, *20*, 2499–2512.
(18) Hau, S. K.; Yip, H.-L.; Jen, A .K.-Y. *Polym. Rev.* **2010**, *50*, 474–510.
(19) De Jong, M. P.; Van IJzendoorn, L. J.; De Voigt, J. A. *Appl. Phys. Lett.* **2000**, *77*, 2255–2257.
(20) Krebs, F. C. *Sol. Energy Mater. Sol. Cells* **2009**, *93*, 465–475.
(21) Chou, C.-H.; Kwan, W. L.; Hong, Z.; Chen, L.-M.; Yang, Y. *Adv. Mater.* **2011**, *23*, 1282–1286.
(22) Ameri, T.; Dennler, G.; Lugnenschmied, C.; Brabec, C. J. *Energy Environ. Sci.* **2009**, *2*, 347–363.
(23) Pegg, L.-J.; Schumann, S.; Hatton, R. A. *ACS Nano* **2010**, *4*, 5671–5678.
(24) Li, G.; Shtotriya, C. V.; Huang, J.; Yang, Y. *Appl. Phys. Lett.* **2006**, *88*, 253503–3.
(25) White, M. S.; Olson, D. C.; Shaheen, S. E.; Kopidakis, N.; Ginley, D. S. *Appl. Phys. Lett.* **2006**, *89*, 143517–3.

(26) Irwin, M. D.; Buchholz, D. B.; Hains, A. W.; Chang, R. P. H.; Marks, T. J. *Proc. Natl. Acad. Sci. U.S.A.* **2008**, *105*, 2783–2787.
(27) Gilot, J.; Barbu, I.; Wienk, M. M.; Janssen, R. A. J. *Appl. Phys. Lett.* **2007**, *91*, 113520–3.
(28) Li, N.; Lassiter, B. E.; Lunt, R. R.; Wei, G.; Forrest, S. R. *Appl. Phys. Lett.* **2009**, *94*, 023307–3.
(29) Yip, H.-L.; Hau, S. K.; Baek, N. S.; Ma, H.; Jen, A. K.-Y. *Adv. Mater.* **2008**, *20*, 2376–2382.
(30) Motiei, L.; Yao, Y.; Choudhury, J.; Yan, H.; Marks, T. J.; Van der Boom, M. E.; Facchetti, A. *J. Am. Chem. Soc.* **2010**, *132*, 12528–12530.
(31) Brabec, C. J.; Shaheen, S. E.; Wnder, C.; Sariciftci, N. S.; Denk, P. *Appl. Phys. Lett.* **2002**, *80*, 1288–1290.
(32) Zhang, F.; Ceder, M.; Inganäs, O. *Adv. Mater.* **2007**, *19*, 1835–1838.
(33) Yuan, Y.; Reece, T. J.; Sharma, P.; Poddar, S.; Ducharme, S.; Gruverman, A.; Yang., Y.; Huang, J. *Nat. Mater.* **2011**, *10*, 296–302.
(34) Ferro, V. R.; Poveda, L. A.; González-Jonte, R. H.; Garcia De La Vega, J. M.; Torres, T.; Del Rey, B. *J. Porphyrins Phthalocyanines* **2000**, *4*, 611–620.
(35) Perez, M. D.; Borek, C.; Forrest, S. R.; Thomson, M. E. *J. Am. Chem. Soc.* **2009**, *131*, 9281–9286.
(36) Pacholski, C.; Kornowski, A.; Weller, H. *Angew. Chem., Int. Ed.* **2002**, *41*, 1188–1191.
(37) Beek, W. J. E.; Wienk, M. M.; Janssen, R. A. J. *J. Mater. Chem.* **2005**, *15*, 2985–2988.
(38) Li, D.; Neumann, A. W. *J. Colloid Interface Sci.* **1990**, *137*, 304–307.
(39) Nilsson, S.; Bernasik, A.; Budkowski, A.; Moons, E. *Macromolecules* **2007**, *40*, 8291–8301.
(40) Pettersson, L. A. A.; Roman, L. S.; Inganäs, O. *J. Appl. Phys.* **1999**, *86*, 487–496.